

Article

Bioactive Monoterpenes and Polyketides from the Ascidian-Derived Fungus *Diaporthe* sp. SYSU-MS4722

Guifa Zhai ^{1,2}, Senhua Chen ^{1,3,*} , Hongjie Shen ^{1,3}, Heng Guo ¹, Minghua Jiang ^{1,3}  and Lan Liu ^{1,3,4,*} ¹ School of Marine Sciences, Sun Yat-sen University, Zhuhai 519000, China² School of Medicine, Shenzhen Campus, Sun Yat-Sen University, Shenzhen 518107, China³ Southern Laboratory of Ocean Science and Engineering (Guangdong, Zhuhai), Zhuhai 519000, China⁴ Pearl River Estuary Marine Ecosystem Research Station, Ministry of Education, Zhuhai 519082, China

* Correspondence: chensenh@mail.sysu.edu.cn (S.C.); cesllan@mail.sysu.edu.cn (L.L.);

Tel.: +86-020-84725459 (S.C. & L.L.)

Abstract: There has been a tremendous increase in the rate of new terpenoids from marine-derived fungi being discovered, while new monoterpenes were rarely isolated from marine-derived fungi in the past two decades. Three new monoterpenes, diaporterpenes A–C (1–3), and one new α -pyrones, diaporpyrone A (6), along with nine known polyketides 4, 5, and 7–13 were isolated from the ascidian-derived fungus *Diaporthe* sp. SYSU-MS4722. Their planar structures were elucidated based on extensive spectroscopic analyses (1D and 2D NMR and HR-ESIMS). The absolute configurations of 1 and 3 were identified by an X-ray crystallographic diffraction experiment using Cu-K α radiation, and those of compound 2 were assigned by calculating NMR chemical shifts and ECD spectra. It afforded an example of natural epimers with different physical properties, especially crystallization, due to the difference in intermolecular hydrogen bonding. Compounds 9, 10, and 13 showed moderate total antioxidant capacity (0.82 of 9; 0.70 of 10; 0.48 of 13) with Trolox (total antioxidant capacity: 1.0) as a positive control, and compounds 5 and 7 showed anti-inflammatory activity with IC₅₀ values of 35.4 and 40.8 μ M, respectively (positive control indomethacin: IC₅₀ = 35.8 μ M).



Citation: Zhai, G.; Chen, S.; Shen, H.; Guo, H.; Jiang, M.; Liu, L. Bioactive Monoterpenes and Polyketides from the Ascidian-Derived Fungus *Diaporthe* sp. SYSU-MS4722. *Mar. Drugs* **2022**, *20*, 553. <https://doi.org/10.3390/md20090553>

Academic Editor: Xian-Wen Yang

Received: 12 August 2022

Accepted: 25 August 2022

Published: 29 August 2022

Publisher's Note: MDPI stays neutral with regard to jurisdictional claims in published maps and institutional affiliations.



Copyright: © 2022 by the authors. Licensee MDPI, Basel, Switzerland. This article is an open access article distributed under the terms and conditions of the Creative Commons Attribution (CC BY) license (<https://creativecommons.org/licenses/by/4.0/>).

Keywords: monoterpenes; α -pyrones; ascidian-derived fungus; *Diaporthe* sp.; antioxidant and anti-inflammatory

1. Introduction

Marine fungal terpenoids are a kind of important metabolites with chemical structural diversity and pharmacological activity, such as cytotoxic, antibacterial, antifungal, antiviral, anti-inflammatory, and enzyme inhibitor activities [1,2]. In the past 20 years, there has been a tremendous increase in the rate of new terpenoids from marine-derived fungi being discovered [1,3,4], while monoterpenes were rarely isolated from marine-derived fungi. Up to now, only 12 new monoterpenes have been obtained from marine-derived fungi, including (1*S*,2*S*,3*S*,4*R*)-3-chloro-4-(2-hydroxypropan-2-yl)-1-methylcyclohexane-1,2-diol [5], pestalotiolactones C and D [6], penicipenes A and B [7], eutypellol B [8], 2-(2-hydroxy-4-methylcyclohex-3-enyl) propanoic acid [8], nectriapyrones C and D [9], (7*S*) and (7*R*)-1-hydroxy-3-*p*-menthen-9-oic acids [10], 1-*O*-(α -D-mannopyranosyl) geraniol [11]. It is a challenging thing to discover new monoterpenes from marine-derived fungi.

The genus *Diaporthe* (asexual state: *Phomopsis*) comprises pathogenic, endophytic and saprobic species with both temperate and tropical distributions [12,13]. Chemical investigation of secondary metabolites and the discovery of novel bioactive natural products have been extensively researched because of their importance as plant pathogens [12]. For example, the mangrove-derived fungus *Diaporthe* sp. SCSIO 41011 produced six new highly oxygenated chloroazaphilone derivatives, isochromophilones A–F, with cytotoxicity [14]. Diaporisoindoles A–C were isolated from the mangrove endophytic fungus *Diaporthe* sp. SYSU-HQ3, which showed significant inhibitory activity against *Mycobacterium tuberculosis*

protein tyrosine phosphatase B [15]. Dihydroisocoumarin, diaporone A, with antibacterial activity, was obtained from an endophytic plant fungus *Diaporthe* sp. [16].

Recently, our research group has focused on the secondary metabolites of ascidian-derived fungi isolated from the South China Sea [17–20]. Twenty mono- and dimeric xanthenes with anti-glioma and anti-inflammatory activities have been obtained from the ascidian-derived fungus *Diaporthe* sp. SYSU-MS4722 [21]. Continuous chemical investigation of the EtOAc extract of marine fungus *Diaporthe* sp. SYSU-MS4722 led to the isolation of three new monoterpenes, diaporterpenes A–C (1–3), and one new α -pyrone, diaporpyrone A (6), along with nine known compounds 4, 5, and 7–13 (Figure 1) Herein, the details of the isolation, structural elucidation, and bioactivity of compounds 1–13 are reported.

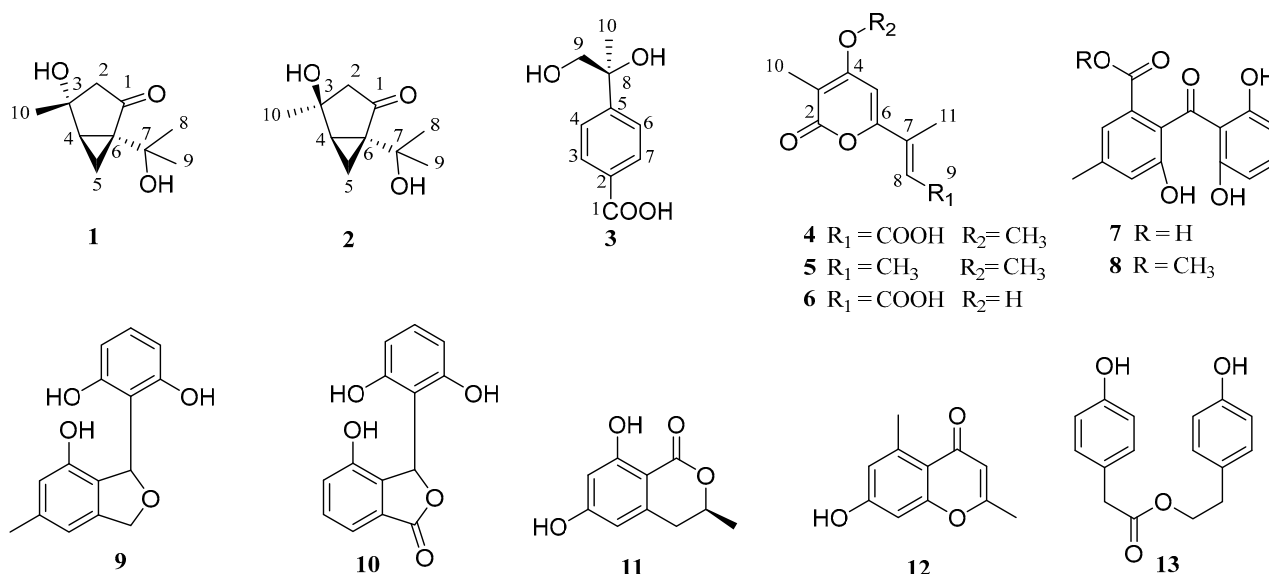


Figure 1. Chemical structures of compounds 1–13.

2. Results and Discussion

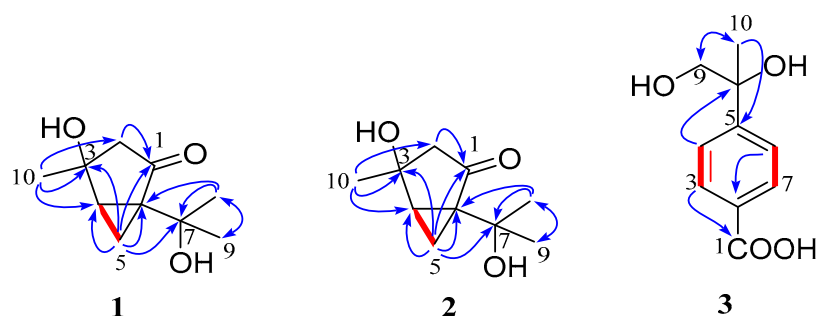
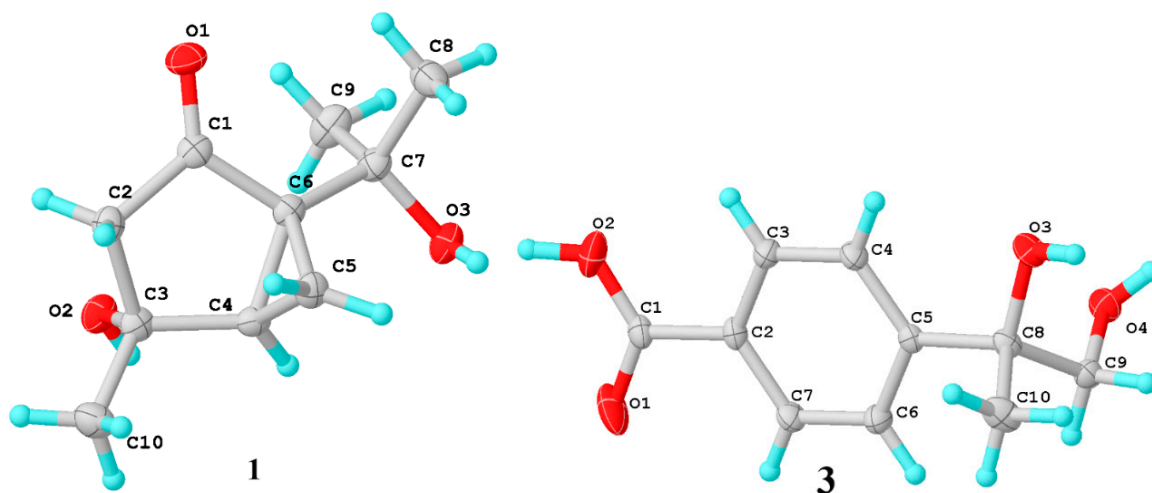
The EtOAc extract of marine-derived fungus *Diaporthe* sp. SYSU-MS4722 was performed on repeated silica gel and Sephadex LH-20 column chromatography, followed by semipreparative HPLC to afford three new monoterpenes, diaporterpenes A–C (1–3), and one new α -pyrone, diaporpyrone A (6), along with nine known polyketides 4, 5, and 7–13.

Diaporterpene A (1) was obtained as a colourless crystal with a melting point of 126–127 °C. The molecular formula was determined as $\text{C}_{10}\text{H}_{16}\text{O}_3$ on the basis of the positive HR-ESIMS ions at m/z 185.1172 $[\text{M} + \text{H}]^+$ (calculated for 185.1172, $\text{C}_{10}\text{H}_{17}\text{O}_3$), implying three degrees of unsaturation. The IR spectrum (Supplementary Figure S8) of 1 revealed the presence of two hydroxy (3399 and 3325 cm^{-1}) groups. The ^1H NMR spectrum (Table 1) of 1 exhibited the signals for three tertiary methyls (δ_{H} 1.32, s; 1.40, s; 1.40, s), two methylenes (δ_{H} 1.97, dd, $J = 0.6, 18.1$ Hz; 2.38, dd, $J = 2.1, 18.1$ Hz; 0.96, dd, $J = 4.6, 4.7$ Hz; 1.48, ddd, $J = 2.1, 5.0, 8.1$ Hz), and one methine (2.23, dd, $J = 4.3, 8.1$ Hz). The ^{13}C NMR and DEPT data (Table 1) of 4 revealed the presence of 10 carbons belonging to one ketone carbonyl group (δ_{C} 214.3), two oxygen-bearing non-hydrogen carbon (δ_{C} 68.9, 73.9), one quaternary carbon (δ_{C} 47.7), one methine (δ_{C} 39.0), two methylenes (δ_{C} 16.1, 50.0), and three methyls (δ_{C} 25.4, 27.2, 27.7). These spectroscopic features suggested that 4 belongs to the family of monoterpenoids and is very similar to 2-thujanone, except for the presence of additional two oxygen-bearing non-hydrogen carbons (δ_{C} 68.9, 73.9) and the absence of two methines.

Table 1. ^1H and ^{13}C NMR spectroscopic data of 1–3 (CD_3OD).

| No. | 1 | | 2 | | 3 | |
|-----|----------------------------|--|----------------------------|---|----------------------------|--------------------------------------|
| | δ_{C} , type | δ_{H} , mult (J in Hz) | δ_{C} , type | δ_{H} , mult (J in Hz) | δ_{C} , type | δ_{H} , mult (J in Hz) |
| 1 | 214.3, C | | 211.9, C | | 170.1, C | |
| 2 | 50.0, CH_2 | 1.97, dd (0.6, 18.1) | 49.6, CH_2 | 1.97, d (17.7) | 108.9, C | |
| 3 | 73.9, C | 2.38, dd (2.1, 18.1) | 71.9, C | 2.44, d (17.7) | | |
| 4 | 39.0, CH | 2.23, dd (4.3, 8.1) | 38.1, CH | 2.24, dd (4.4, 7.8) | 130.4, CH | 7.88, d (8.4) |
| 5 | 16.1, CH_2 | 0.96, dd (4.6, 4.7) 1.48, ddd (2.1, 5.0 8.1) | 15.7, CH_2 | 1.32, dd (4.6, 4.7) 1.52, ddd (1.6, 4.8, 7.6) | 126.7, CH | 7.49, d (8.4) |
| 6 | 47.7, C | | 50.3, C | | 152.9, C | |
| 7 | 68.9, C | | 68.5, C | | 126.7, CH | 7.49, d (8.4) |
| 8 | 27.2, CH_3 | 1.32, s | 29.2, CH_3 | 1.28, s | 130.4, CH | 7.88, d (8.4) |
| 9 | 27.8, CH_3 | 1.40, s | 28.0, CH_3 | 1.39, s | 75.7, C | |
| 10 | 25.6, CH_3 | 1.40, s | 27.2, CH_3 | 1.41, s | 71.6, CH_2 | 3.52, q (11.2) |
| | | | | | 26.0, CH_3 | 1.42, s |

The planar structure was further assigned by 2D NMR spectra (^1H - ^1H COSY, HSQC, HMBC) (Figure 2). The key HMBC correlations from H-2 to ketone C-1, from H-10 to C-2, C-3, C-4, from H-5 to C-2, C-3, C-4, C-6, C-7, and from H-8 and H-9 to C-6 and C-7, as well as ^1H - ^1H COSY of H-4/H-5/H-6, indicated the presence of 1-isopropyl-4-methylbicyclo [3.1.0]hexan-2-one structure (2-thujanone). In the light of the chemical shifts (δ_{C} 73.9, C-3; 68.9, C-7), the remaining hydroxyl groups were located on C-3 and C-7, respectively. The absolute configuration of 1 was assigned as (3*R*,4*R*,6*S*) by a single-crystal X-ray diffraction experiment using Cu-K α radiation (Figure 3) (Flack parameter = 0.09(19)).

**Figure 2.** Key ^1H - ^1H COSY (red line) and HMBC (blue arrow) correlations of compounds 1–3.**Figure 3.** X-ray crystallographic analysis of 1 and 3.

Diaporterpene B (**2**) was obtained as a colorless oil, and its molecular formula was identified as the same as **1** with $C_{10}H_{16}O_3$ by the negative HRESIMS ions at m/z 183.1025 $[M - H]^-$ (calculated for 183.1026, $C_{10}H_{15}O_3$). Compound **2** shared the same planar structure as **1** and was further identified by 2D NMR spectra, including 1H - 1H COSY, HSQC, and HMBC (Figure 2). The minor chemical shift variation of C-3 (δ_C 73.9 for **1**; δ_C 71.9 for **2**), C-5 (δ_C 16.1, δ_H 1.48 for **1**; δ_C 15.7, δ_H 1.52 for **2**), C-10 (δ_C 25.6, δ_H 1.40 for **1**; δ_C 27.2, δ_H 1.40 for **2**) were observed in same CD_3OD solvent; this suggested that **2** should be a 3-epimer of **1**. The relative configuration of **2** was determined by analysis of the NOESY data's difference between **1** and **2** (Figures S7 and S14). The additional presence of a NOESY correlation between H-10 and H-4 and the absence of NOESY correlation between H-10 and H-2 α and H-5 α in **2** indicated that H-10 and H-4 were the same facial sides (Figure 4). In order to determine the epimer relationship between **1** and **2**, the ^{13}C NMR calculations of **1** (3-*epi*-**2**) and **2** at the B3LYP/6-311++G(2d,p) level were performed. The calculated NMR chemical shifts of **2** (3*S*, 4*R*, 6*S*) agreed better with the experimental data compared to those of 3-*epi*-**2** (3*R*, 4*R*, 6*S*) (Figure 5 and Figure S32). The DP4 probability analysis also revealed that **2** had 100% probability, while it had 0% probability for **1** (Figure S33). Finally, the absolute configuration was deduced by comparing experimental and calculated ECD spectra (Figure 6). The predicted ECD spectrum of (3*S*,4*R*,6*S*)-**2** was in good agreement with the experimental one. Thus, the absolute configuration of **2** was assigned as 3*S*,4*R*,6*S*.

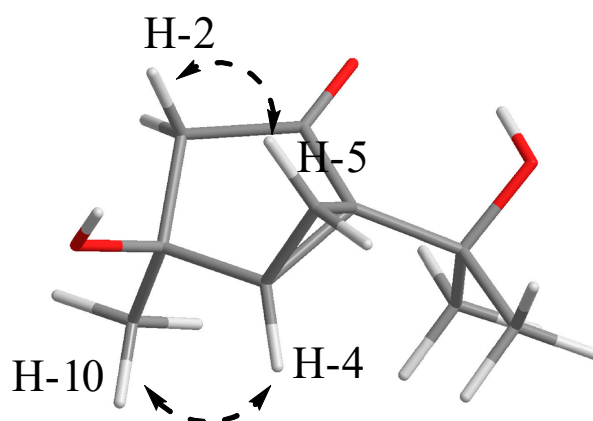


Figure 4. Key NOE (dash arrow) correlations of compound **2**.

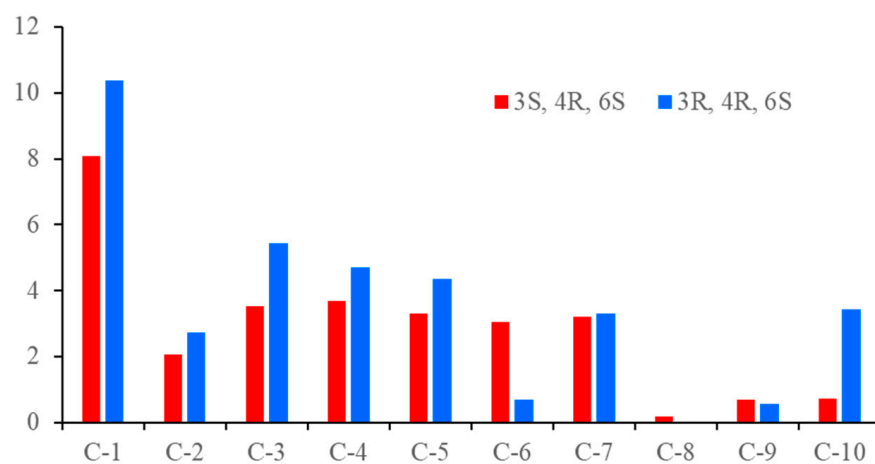


Figure 5. Values of the absolute deviation ($|\Delta\delta| = |\delta_{\text{calcd}} - \delta_{\text{exptl}}|$) for the possible structure of **2**.

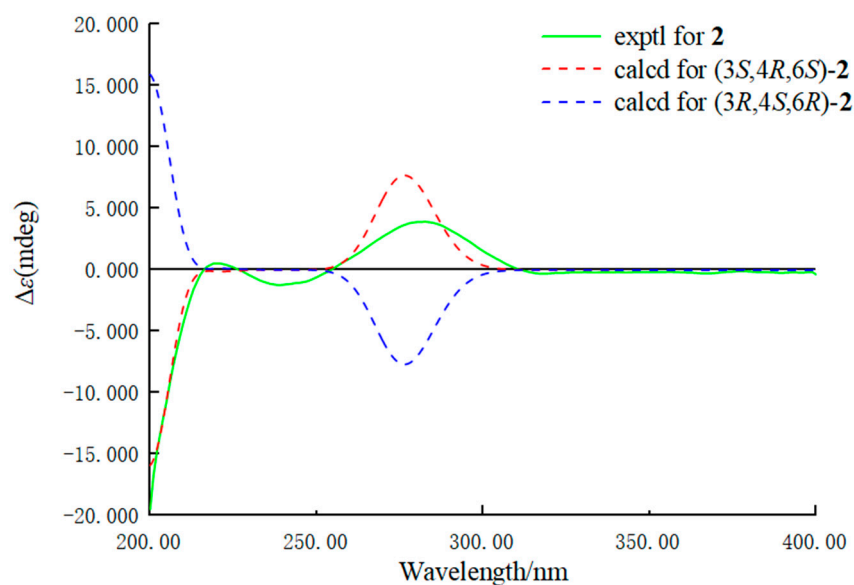


Figure 6. Experimental and predicted ECD spectra of **2** (in MeOH).

The monoterpenes, diaporterpenes A and B, were a pair of epimers with different physical properties, especially crystallization and solid-liquid states. Diaporterpene A was a solid state and had easy crystallization properties, while diaporterpene B was a liquid state and had difficult crystallization properties. Analysis of single crystal structure and molecular packing properties of **1** (Figure 7), intermolecular hydrogen bonds were observed. The 3-OH and 7-OH were the key functional groups for forming the intermolecular hydrogen bonds, while the O atom of the ketone does not make contributions. One molecule and four molecules around it together form five hydrogen bonding and look like a door handle. This is the main reason for the easy crystallization property for **1**. However, the absolute configuration of 3-OH in **2** was *S* with opposite orientation compared to **1**, which led to difficulty forming intermolecular hydrogen.

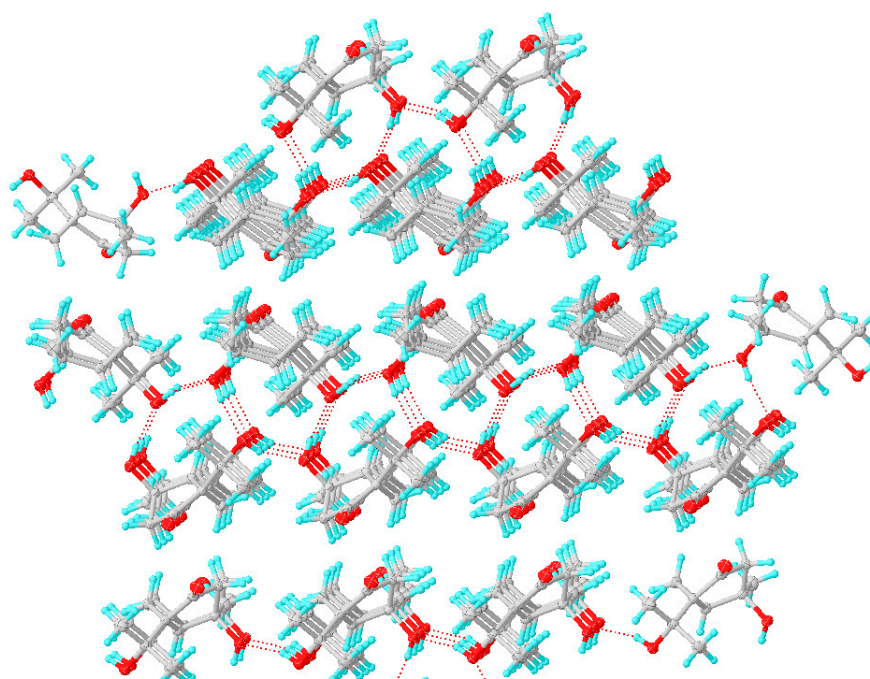


Figure 7. Single crystal molecular packing properties of **1**.

Diaporterpene C (**3**) was obtained as a colourless crystal. The molecular formula was determined as $C_{10}H_{12}O_4$ on the basis of the negative HR-ESIMS ions at m/z 195.0666 $[M - H]^-$ (calculated for 195.0663, $C_{10}H_{11}O_4$), implying five degrees of unsaturation. The 1H NMR data (Table 1) revealed resonances for four para-substituted aromatic protons (δ_H 7.49 (2H, dd, $J = 8.4$ Hz); 7.88 (2H, d, $J = 8.4$ Hz)), one hydroxymethyl (δ_H 3.52 (2H, q, $J = 11.2$ Hz)), and one tertiary methyl (δ_H 1.42, s). The ^{13}C NMR and DEPT data (Table 1) of 5 revealed the presence of 10 carbons which were assigned with the help of an HSQC experiment. Except for seven sp^2 hybridized carbons (δ_C 108.9, 130.4, 126.7, 152.9, 126.7, 130.4, 170.1) belonging to one benzoic acid, the remaining three sp^3 hybridized carbons were sorted as methyl (δ_C 26.0), methylene (δ_C 71.6), and an oxygen-bearing non-hydrogen carbon (δ_C 75.7). The HMBC correlations from methyl H-10 and hydroxymethyl H-9 to C-8 and C-5 of benzoic acid indicated a methyl, a hydroxymethyl, and a hydroxyl were all connected to C-7 that was directly linked to C-5 of benzoic acid. Finally, the absolute configuration of **3** was assigned as *S* by a single-crystal X-ray diffraction experiment using Cu-K α radiation (Flack parameter = $-0.08(15)$) (Figure 3).

Diaporpyrone A (**6**) was obtained as a white powder, and its molecular formula $C_{10}H_{10}O_5$ was established by the positive HRESIMS ion at m/z 209.0452 $[M - H]^-$ (calculated for $C_{10}H_9O_5$, 209.0455) showing six degrees of unsaturation. The 1H NMR spectrum displayed two olefinic protons at δ_H 6.45 (s) and 6.60 (d, $J = 1.3$ Hz) and two methyls (δ_H 1.88, s, and 2.88, s). The ^{13}C NMR spectrum showed 10 carbons, including two conjugated carbonyls (δ_C 167.2, 169.8), six olefinic carbons (102.8, 103.3, 121.4, 142.7, 158.1, 166.8), and two sp^3 carbons (8.7, 13.7). The key HMBC correlations of H-10 to C-2, C-3, and C-4, and H-5 to C-3, C-4, and C-6 suggested the presence of an α -pyrone moiety with a methyl substituent at C-3 (Figure 8). The HMBC correlations from H-11 to C-7 and H-8 to C-9 assigned a but-2-enoic acid moiety, which was connected to α -pyrone moiety via C-6. Key NOE correlation between H-5 with H-11 indicated that H-5 and H-11 were on the same side, while NOE correlation between H-8 with H-11 was not observed, suggesting that H-8 with H-11 were in the trans position. Hence, compound **6** was identified as shown in Figure 8.

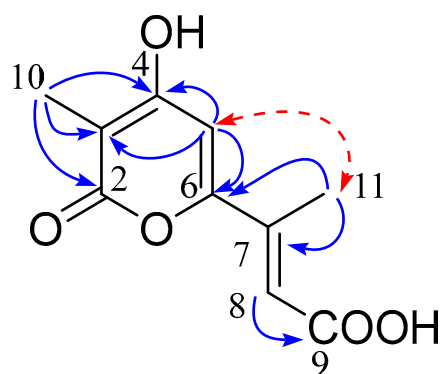


Figure 8. Key HMBC (blue arrow) and NOE (red dash arrow) correlations of compound **6**.

The known isolates were identified as acropyrone (**4**) [22], nectriapyrone (**5**) [23], monodictyphenone (**7**) [24], 2,2',6'-trihydroxy-4-methyl-6-methoxy-acyl-diphenylmethanone (**8**) [25], pestacin (**9**) [26], 3-(2,6-dihydroxyphenyl)-4-hydroxy-6-methyl-isobenzofuran-1(3*H*)-one (**10**) [27], 3,4-dihydro-6,8-dihydroxy-3-methylisocoumarin (**11**) [28], 2,5-dimethyl-7-hydroxychromone (**12**) [25], and 4-hydroxyphenethyl 2-(4-hydroxyphenyl) acetate (**13**) [29] by comparison of their spectroscopic data with those reported in the literature.

Phenolic compounds (including cinnamic acids, benzoic acids, flavonoids, proanthocyanidins, coumarins, stilbenes, lignans, and lignins) are the most widespread class of metabolites in nature and are proven to be effective antioxidants [30]. Compounds **1–13** were evaluated using the total antioxidant capacity assay kit with a rapid ABTS method. Only compounds **9**, **10**, and **13** showed moderate total antioxidant capacity (0.82 of **9**;

0.70 of **10**; 0.48 of **13**) with Trolox as a positive control. Anti-inflammatory activities were performed for compounds **1–13** with the inhibition of nitric oxide (NO) production in RAW264.7 cells activated by lipopolysaccharides, and compounds **5** and **7** showed anti-inflammatory activity with IC_{50} values 35.4 and 40.8 μ M, respectively, with indomethacin ($IC_{50} = 35.8 \mu$ M) as a positive control. All isolates were evaluated for anti-glioma activity using T98G human cell line with temozolomide as the positive control, and none of them showed significant cytotoxicity against T98G human cell line.

3. Materials and Methods

3.1. General Experimental Procedures

Optical rotations were carried out on an MCP-200 polarimeter (Anton Paar, Graz, Austria) with MeOH as solvent at 25 °C. UV spectra were acquired on a Blue Star A spectrophotometer. IR data were performed on a Fourier transformation infrared spectrometer coupled with an EQUINOX 55 infrared microscope (Bruker, Fällanden, Switzerland). Here, 1D and 2D NMR spectra were tested on a Bruker Avance 400 MHz spectrometer (Bruker, Fällanden, Switzerland) using TMS as an internal standard. HRESIMS and ESIMS data were recorded on an LTQ-Orbitrap LC-MS spectrometer (Thermo Corporation, MA, USA) and an ACQUITY QDA (Waters Corporation, MA, USA), respectively. HPLC preparative separations were performed on a Shimadzu Essentia LC-16. The Welch-Ultimate XB-C18 column (250 × 21.2 mm, 5 μ m, 12 nm, Welch Materials, Inc., Shanghai, China) was used for preparative HPLC. Semi-preparative HPLC separations were performed on ACE-5-C18-AR and ACE-5-CN-ES columns (250 × 10 mm, 5 μ m, 12 nm, Advanced Chromatography Technologies Ltd., Guangzhou, China). The silica gel (200–300 mesh, Qingdao Marine Chemical Inc., Qingdao, China) and Sephadex LH-20 (Amersham Biosciences, Uppsala, Sweden) were subjected to column chromatography (CC).

3.2. Fungal Material

The detail of the fungus was described previously [21]. The molecular biological protocol, including DNA amplification and sequencing of the ITS region, was used for fungal identification. The sequence data of the fungal strain have been deposited at GenBank with accession no. OK623372. A BLAST search result suggested that the sequence was most similar (100%) to the sequence of *Diaporthe* sp. NFIF-2-6 (compared to MW202988.1). The strain was preserved at the School of Marine Sciences, Sun Yat-Sen University.

3.3. Extraction and Isolation

The strain *Diaporthe* sp. SYSU-MS4722 was grown on a solid rice medium in a 1000 mL culture flask containing 50g of rice and 50 mL of 3% artificial seawater after sterilization. A total of 120 flasks of fungal incubation were cultivated at room temperature for 30 days. The solid fermented substrate was extracted with MeOH four times to obtain a crude extract, then dissolved in H₂O and continuously extracted four times with EtOAc solvent. The EtOAc extract (42 g) was subjected to a silica gel column eluting with linear gradient petroleum ether/EtOAc (from 8:2 to 0:1) to obtain six fractions (A–F).

Fr.A was chromatographed on a Sephadex LH-20 column with MeOH/CH₂Cl₂ (50:50) to afford three fractions (Fr.A.1 to Fr.A.3) and compounds **9** and **13**. Fr.B was applied to the Sephadex LH-20 column with CH₂Cl₂/MeOH to provide four subfractions (Fr.B.1 to Fr.B.4). Fr.B.1 was further subjected to RP-HPLC (MeOH /H₂O, 80:20 flow rate 2 mL/min, ACE-C18-PFP column 10 × 250 mm, 5 μ m) to afford **11** (6.0 mg, $t_R = 17.6$ min). Fr.B.4 was applied to a silica gel column with CH₂Cl₂/MeOH (98:2) and then purified by RP-HPLC with MeOH/H₂O (70:30) to give **12** (2 mg, $t_R = 16.4$ min). Fr.C was separated by a silica gel column eluting with CH₂Cl₂/MeOH (97:3) to afford five fractions (Fr.C.4.1 to Fr.C.4.5) and compound **8**. Fr.C.4.2 was further purified by a Sephadex LH-20 column with CH₂Cl₂/MeOH to give **4** (9.0 mg). Fr.C.4.3 was further purified by a silica gel column to give **5** (5.9 mg). Compounds **2** (20 mg, $t_R = 13.4$ min) were obtained from Fr.C.4.3 by silica gel CC (CH₂Cl₂/MeOH, 50:1, 30:1, 20:1, 10:1, v/v) with a final purification on a

XB-C18 column (Welch column, MeCN/H₂O, 14:86, 12 mL·min⁻¹). Fr.C.4.5 was further purified by silica gel column to three fractions (Fr.C.4.5.1 to Fr.C.4.5.3), and Fr.C.4.5.2 was further purified by RP-HPLC (MeOH /H₂O, 65:35 flow rate 2 mL/min, ACE-C18-PFP column 10 × 250 mm, 5 μm) to give **10** (9.0 mg, *t_R* = 10.8 min). Fr.C.4.5.3 was further purified by RP-HPLC (MeOH /H₂O, 65:35 flow rate 2 mL/min, ACE-C18-PFP column 10 × 250 mm, 5 μm) to give **7** (9.0 mg). Fr.C.5 was subjected to silica gel chromatography to afford **6** (11 mg) and Fr.C.5.2, which was further purified by RP-HPLC (MeOH/H₂O, 60:40 flow rate 2 mL/min, ACE-C18-PFP column 10 × 250 mm, 5 μm) to give **1** (5.0 mg, *t_R* = 14.6 min). Fr.C.4.5 was further fractionated on a silica gel column and RP-HPLC to afford **3** (12 mg, *t_R* = 19.5 min).

Compound 1: Colourless crystal; mp 126–127 °C; $[\alpha]_D^{20}$ -1.5 (*c* 1.00, MeOH); UV (MeOH) λ_{\max} (log ϵ) 203 (3.48) nm; IR (neat) ν_{\max} 3399, 3325, 2971, 2933, 1714, 1457, 1371, 1312, 1271, 1151, 1092, 928, 857 cm⁻¹; HRESIMS *m/z* 185.1172 [M - H]⁺ (calculated for C₁₀H₁₅O₃, 185.1172).

Compound 2: brown oil; $[\alpha]_D^{20}$ -5.3 (*c* 1.00, MeOH); UV (MeOH) λ_{\max} (log ϵ) 203 (3.48) nm; CD $\Delta\epsilon$ (0.5 mg/mL, MeOH) λ_{\max} ($\Delta\epsilon$) 218 (0.79), 240 (-1.15), 283 (3.98) nm; IR (neat) ν_{\max} 3400, 2970, 2931, 1707, 1456, 1375, 1307, 1267, 1134, 1097, 1020, 947, 860 cm⁻¹; ¹H and ¹³C NMR data, see Table 2; HRESIMS *m/z* 183.10251 [M - H]⁻ (calculated for C₁₀H₁₅O₃, 183.10267).

Table 2. ¹H (400 MHz) and ¹³C (100 MHz) NMR spectroscopic data of **6** (CD₃OD).

| No. | 6 | |
|-----|-----------------------|-----------------------------|
| | δ_C , type | δ_H , mult (J in Hz) |
| 2 | 167.2, C | |
| 3 | 102.8, C | |
| 4 | 166.8, C | |
| 5 | 103.3, CH | 6.45, s |
| 6 | 158.1, C | |
| 7 | 142.7, C | |
| 8 | 121.4, CH | 6.60, d (1.3) |
| 9 | 169.7, C | |
| 10 | 8.7, CH ₃ | 1.88, s |
| 11 | 13.5, CH ₃ | 2.30, s |
| 12 | OH | |

Compound 3: Colourless crystal; mp 133–135 °C; UV (MeOH) λ_{\max} (log ϵ) 232 (3.87) nm; IR (neat) ν_{\max} 3388, 1703, 1620, 1414, 1277, 1049 cm⁻¹; HR-ESIMS *m/z* 195.0666 [M - H]⁻ (calculated for C₁₀H₁₁O₄, 195.0663).

Compound 6: Colourless powder; UV (MeOH) λ_{\max} (log ϵ) 213 (4.05), 232 (3.89), 331 (3.93) nm; IR (neat) ν_{\max} 3215, 1668, 1585, 1416, 1254, 1076 cm⁻¹; HR-ESIMS *m/z* 209.0452 [M - H]⁻ (calculated for C₁₀H₉O₅, 209.0455).

3.4. X-ray Crystallographic Analysis

Compounds **1** and **3** were obtained as colorless crystals using the vapor diffusion method. The single crystal X-ray diffraction data were recorded on a Rigaku Oxford Diffraction with Cu-K α radiation (λ = 1.54178 Å). The structures were solved by direct methods (SHELXS-97 and Olex2-1.2) and refined using full-matrix least-squares difference Fourier techniques. Crystallographic data for **1** and **3** have been deposited with the Cambridge Crystallographic Data Centre. Copies of the data can be obtained, free of charge, on application to the Director, CCDC, 12 Union Road, Cambridge CB2 1EZ, UK (fax: 44-(0)1223-336033, or e-mail: deposit@ccdc.cam.ac.uk).

Compound 1: C₁₀H₁₆O₃ (*M_r* = 184.23 g/mol), orthorhombic, space group P2₁2₁2₁, *a* = 6.5845(2) Å, *b* = 7.8419(2) Å, *c* = 20.0925(6) Å, α = 90°, β = 90°, γ = 90°, *V* = 1037.48(5) Å³, *Z* = 4, *T* = 249.99(10) K, μ (Cu K α) = 0.702 mm⁻¹, *D*_{calc} = 1.179 g/cm³; 2039 reflections

measured ($R_{\text{int}} = 0.0387$, $R_{\text{sigma}} = 0.0581$), which were used in all calculations. The final R_1 was 0.0402 ($I \geq 2u(I)$), and wR_2 was 0.1031. The Flack parameter was 0.09(19). The goodness of fit on F^2 was 1.053. CCDC 1997240.

Compound **3**: $\text{C}_{10}\text{H}_{12}\text{O}_4$ ($M_r = 196.20$ g/mol), tetragonal, space group $P4_32_12$, $a = 7.03910(10)$ Å, $b = 7.03910(10)$ Å, $c = 37.3747(6)$ Å, $\alpha = 90$, $\beta = 90$, $\gamma = 90$, $V = 1851.88(6)$ Å³, $Z = 8$, Crystal size $0.3 \times 0.2 \times 0.05$ mm³, $\mu(\text{Cu K}\alpha) = 0.917$ mm⁻¹, $D_{\text{calc}} = 1.407$ g/cm³; 1874 reflections were measured ($R_{\text{int}} = 0.0467$, $R_{\text{sigma}} = 0.0366$), which were used in all calculations. The final R_1 was 0.0440 ($I \geq 2u(I)$), and wR_2 was 0.1206. The Flack parameter was $-0.08(15)$. The goodness of fit on F^2 was 1.059. CCDC 1997237.

3.5. Calculation of the ECD Spectra

Merck molecular force field (MMFF) and DFT/TD-DFT calculations were performed with the Spartan'14 software package (Wavefunction Inc., Irvine, CA, USA) and the Gaussian 09 program (Gaussian, Inc., Wallingford, CT, USA), respectively [31]. MMFF conformational search generated low-energy conformers within a 10 kcal·mol⁻¹ energy window. All the lowest energy conformers were subjected to DFT geometry optimizations at the $\omega\text{B97X-D}$ [32]/TZVP [33] level with the solvation model PCM for methanol. Frequency calculations were performed at the same level to confirm that each optimized conformer was at its true minimum and to estimate their relative thermal free energies (ΔG) at 298.15 K. Single-point energies were calculated at the M06-2X [34]/def2-TZVP [35]/SDM(MeOH) level of theory. The population of each conformer was calculated by Boltzmann distribution based on Gibbs free energy with the Shermo [36]. Finally, a free energy correction +1.89 kcal·mol⁻¹ was applied to all free energies to consider the conversion from the gas phase (1 atm) to the liquid phase (1 M). Then, conformers with distributions higher than 1% were chosen for the TDDFT calculations at the PBE1PBE/TZVP [33] level in methanol. The ECD spectrum was generated by the program SpecDis [37] using a Gaussian band shape with 0.20 eV exponential half-width from dipole-length dipolar and rotational strengths. NMR calculations used the gauge-including atomic orbitals (GIAO) method at the mPW1PW91/6-311+G(d,p) level in MeOH simulated by the IEFPCM model. The TMS-corrected NMR chemical shift values were averaged according to Boltzmann distribution and fitted to the experimental values by linear regression. To confirm the conclusions of NMR calculations, DP4+ analysis was also performed. All calculations were performed by Tianhe-2 in National Super Computer Center in Guangzhou.

3.6. Anti-Glioma Activity

The assays for anti-glioma activity were evaluated as described previously [21]. The human glioma cell line, T98G, was purchased from the Cell Bank of the Chinese Academy of Sciences. Cells were cultured in Dulbecco's modified Eagle's medium (DMEM, Gibco, Carlsbad, CA, USA), containing 10% fetal bovine serum (FBS), 100 IU/mL penicillin, and 100 µg/mL streptomycin (all from Gibco, Carlsbad, CA, USA) in a cell incubator with 5% CO₂ at 37 °C.

Cell proliferation was analyzed by MTT according to the manufacturer's instructions. Briefly, T98G was digested and seeded at 1×10^3 cells/well in 96-well plates and cultured in a 100 µL medium overnight. The cells were treated with tested compounds with gradient concentrations for 48 h. At each indicated time point, MTT solution (10 µL/well) was added and then incubated at 37 °C for 2 h. The optical density (OD) at 450 nm was recorded by a microplate reader (Multiskan GO, Thermo Scientific, Waltham, MA, USA). Each experiment was performed three times.

3.7. Anti-Inflammatory Activity

The assays for anti-inflammatory activity were performed as described previously [38]. RAW 264.7 cells were seeded in 96-well plates at a density of 5×10^5 cells/mL. After 12 h, the cells were treated with 1 µg/mL of LPS and tested samples, followed by additional incubation for 24 h at 37 °C. MTT stock solution (2 mg/mL) was added to wells for a total

reaction volume of 100 μ L. After 4 h incubation, the supernatants were aspirated. The formazan crystals in each well were dissolved in DMSO (100 μ L), and the absorbance was measured with the wavelength of 490 nm by a microplate reader (Multiskan GO, Thermo Scientific). The data were expressed as mean percentages of the viable cells compared to the respective control. After pre-incubation of RAW 264.7 cells (1.5×10^5 cells/mL) with 1 μ g/mL LPS and samples at 37 °C for 24 h, the quantity of nitrite accumulated in the culture medium was measured as an indicator of NO production. Briefly, cell culture medium (50 μ L) was added with Griess reagent (100 μ L) and incubated at room temperature for 10 min. The absorbance was measured by a microplate reader (Multiskan GO, Thermo Scientific, Waltham, MA, USA) at 540 nm wavelength.

3.8. Total Antioxidant Capacity Assay

The assays for total antioxidant capacity were carried out as described previously [18]. A total antioxidant capacity assay kit with a rapid ABTS method (Beyotime Institute of Biotechnology, Shanghai, China) was used to evaluate the total antioxidant capacity based on the manufacturer's instructions. Samples were incubated at 25 °C for 6 min and then were recorded at 414 nm using a multimode reader (Thermo Fisher Scientific, Waltham, MA, USA).

4. Conclusions

It is a challenging thing to discover new monoterpenes from marine-derived fungi. Continuous chemical investigation of the EtOAc extract of marine fungus *Diaporthe* sp. SYSU-MS4722 afforded three new monoterpenes, diaporterpenes A–C (1–3), and one new α -pyrone, diaporpyrone A (6), along with nine known polyketides. Compounds 9, 10, and 13 showed moderate total antioxidant capacity (0.82 of 9; 0.70 of 10; 0.48 of 13) with Trolox as a positive control, and compounds 5 and 7 showed anti-inflammatory activity with IC₅₀ values of 35.4 and 40.8 μ M, respectively. It afforded an example of natural epimers with different physical properties, especially crystallization, due to the difference in intermolecular hydrogen bonding.

Supplementary Materials: The following are available online at <https://www.mdpi.com/article/10.3390/md20090553/s1>, Figure S1: The HRESIMS spectrum of compound 1, Figures S2–S7: The 1 and 2D NMR (400MHz) spectra of compound 1 in CD₃OD, Figure S8: The IR spectrum of compound 1, Figure S9: The HRESIMS spectrum of compound 2, Figure S10–S15: The 1 and 2D NMR (600MHz) spectra of compound 2 in CD₃OD, Figure S16: The IR spectrum of compound 2, Figure S17–S22: The 2D NMR (400MHz) spectra of compound 3 in CD₃OD, Figure S23: The IR spectrum of compound 3, Figure S24: The HRESIMS spectrum of compound 6, Figure S25–S30: The 1 and 2D NMR (400MHz) spectra of compound 6 in CD₃OD, Figure S31: The IR spectrum of compound 6. Figure S32. Linear correlation between the experimental ¹³C NMR chemical shifts for 2. Figure S33. The DP4 probability analysis. Table S1. Energy of all conformers of compound 2. Figure S34. wB97XD/TZVP optimized low-energy conformers of compound 2. Table S2. Cartesian coordinates of the low-energy reoptimized conformers of 2 calculated at PBE1PBE/TZVP level of theory in IEFPCM for methanol.

Author Contributions: Conceptualization, S.C. and L.L.; methodology, S.C. and H.G.; data analysis, M.J., H.G. and S.C.; experiment, H.S. and G.Z.; resources, writing—original draft preparation, S.C. and G.Z.; writing—review and editing, S.C.; funding acquisition, S.C. and L.L. All authors have read and agreed to the published version of the manuscript.

Funding: This work was supported by the National Natural Science Foundation of China (Grant No. U20A2001, 41806155), Guangdong Marine Economy Development Special Project (No. GDNRC [2022]35), the 2022 Open Foundation of Key Laboratory of Tropical Medicinal Plant Chemistry of Ministry of Education (RDZH2022004), and the Fundamental Research Funds for the Central Universities, Sun Yat-Sen University (22qntd2202).

Institutional Review Board Statement: Not applicable.

Informed Consent Statement: Not applicable.

Acknowledgments: We acknowledge the staff of the Instrumental Analysis and Research Center (Ling Fang, Xinhai Zhu, et al.) at Sun Yat-Sen University and the analytical facilities (Aijun Sun, Xuan Ma, et al.) at SCSIO for helping us to finish the spectra test.

Conflicts of Interest: The authors declare no conflict of interest.

References

1. Jiang, M.; Wu, Z.; Guo, H.; Liu, L.; Chen, S. A Review of terpenes from marine-derived fungi: 2015–2019. *Mar. Drugs* **2020**, *18*, 321. [[CrossRef](#)]
2. Chen, S.; Cai, R.; Liu, Z.; Cui, H.; She, Z. Secondary metabolites from mangrove-associated fungi: Source, chemistry and bioactivities. *Nat. Prod. Rep.* **2022**, *39*, 560–595. [[CrossRef](#)]
3. Elissawy, A.M.; El-Shazly, M.; Ebada, S.S.; Singab, A.B.; Proksch, P. Bioactive terpenes from marine-derived fungi. *Mar. Drugs* **2015**, *13*, 1966–1992. [[CrossRef](#)] [[PubMed](#)]
4. Ebel, R. Terpenes from marine-derived fungi. *Mar. Drugs* **2010**, *8*, 2340–2368. [[CrossRef](#)]
5. Huang, H.-R.; Xia, X.-K.; She, Z.-G.; Lin, Y.-C.; Vrijmoed, L.; Gareth Jones, E. A new chloro-monoterpene from the mangrove endophytic fungus *Tryblidiopycnis* sp. (4275). *J. Asian Nat. Prod. Res.* **2006**, *8*, 609–612. [[CrossRef](#)]
6. Li, X.-D.; Li, X.-M.; Yin, X.-L.; Li, X.; Wang, B.-G. Antimicrobial sesquiterpenoid derivatives and monoterpenoids from the deep-sea sediment-derived fungus *Aspergillus versicolor* SD-330. *Mar. Drugs* **2019**, *17*, 563. [[CrossRef](#)]
7. Cheng, Z.; Xu, W.; Wang, Y.; Bai, S.; Liu, L.; Luo, Z.; Yuan, W.; Li, Q. Two new meroterpenoids and two new monoterpenoids from the deep sea-derived fungus *Penicillium* sp. YPGA11. *Fitoterapia* **2019**, *133*, 120–124. [[CrossRef](#)]
8. Liu, H.-X.; Zhang, L.; Chen, Y.-C.; Sun, Z.-H.; Pan, Q.-L.; Li, H.-H.; Zhang, W.-M. Monoterpenes and sesquiterpenes from the marine sediment-derived fungus *Eutypella scoparia* FS46. *J. Asian Nat. Prod. Res.* **2017**, *19*, 145–151. [[CrossRef](#)]
9. Gong, T.; Zhen, X.; Li, B.-J.; Yang, J.-L.; Zhu, P. Two new monoterpene α -pyrones from a fungus *Nectria* sp. HLS206 associated with the marine sponge *Gelliodes carnosa*. *J. Asian Nat. Prod. Res.* **2015**, *17*, 633–637. [[CrossRef](#)]
10. Song, Y.-P.; Miao, F.-P.; Fang, S.-T.; Yin, X.-L.; Ji, N.-Y. Halogenated and nonhalogenated metabolites from the marine-alga-endophytic fungus *Trichoderma asperellum* cf44-2. *Mar. Drugs* **2018**, *16*, 266. [[CrossRef](#)]
11. Yun, K.; Kondempudi, C.M.; Leutou, A.S.; Son, B.W. New Production of a Monoterpene Glycoside, 1-O-(α -D-Mannopyranosyl) geraniol, by the Marine-derived Fungus *Thielavia hyalocarpa*. *Bull. Korean Chem. Soc.* **2015**, *36*, 2391–2393. [[CrossRef](#)]
12. Chepkirui, C.; Stadler, M. The genus *Diaporthe*: A rich source of diverse and bioactive metabolites. *Mycol. Prog.* **2017**, *16*, 477–494. [[CrossRef](#)]
13. Huang, F.; Hou, X.; Dewdney, M.M.; Fu, Y.; Chen, G.; Hyde, K.D.; Li, H. *Diaporthe* species occurring on citrus in China. *Fung. Divers.* **2013**, *61*, 237–250. [[CrossRef](#)]
14. Luo, X.; Lin, X.; Tao, H.; Wang, J.; Li, J.; Yang, B.; Zhou, X.; Liu, Y. Isochromophilones A–F, Cytotoxic Chloroazaphilones from the Marine Mangrove Endophytic Fungus *Diaporthe* sp. SCSIO 41011. *J. Nat. Prod.* **2018**, *81*, 934–941. [[CrossRef](#)]
15. Cui, H.; Lin, Y.; Luo, M.; Lu, Y.; Huang, X.; She, Z. Diaporisoindoles A–C: Three isoprenylisoindole alkaloid derivatives from the mangrove endophytic fungus *Diaporthe* sp. SYSU-HQ3. *Org. Lett.* **2017**, *19*, 5621–5624. [[CrossRef](#)]
16. Guo, L.; Niu, S.; Chen, S.; Liu, L. Diaporone A, a new antibacterial secondary metabolite from the plant endophytic fungus *Diaporthe* sp. *J. Antibiot.* **2020**, *73*, 116–119. [[CrossRef](#)]
17. Chen, S.; Shen, H.; Zhang, P.; Cheng, H.; Dai, X.; Liu, L. Anti-glioma trichobamide A with an unprecedented tetrahydro-5H-furo [2,3-b]pyrrol-5-one functionality from ascidian-derived fungus *Trichobotrys effuse* 4729. *Chem. Commun.* **2019**, *55*, 1438–1441. [[CrossRef](#)]
18. Chen, S.; Shen, H.; Deng, Y.; Guo, H.; Jiang, M.; Wu, Z.; Yin, H.; Liu, L. Rousoelins A and B: Two phenols with antioxidant capacity from ascidian-derived fungus *Rousoella siamensis* SYSU-MS4723. *Mar. Life Sci. Technol.* **2021**, *3*, 69–76. [[CrossRef](#)]
19. Jiang, M.; Wu, Z.; Wu, Q.; Yin, H.; Guo, H.; Yuan, S.; Liu, Z.; Chen, S.; Liu, L. Amphichoterpenoids A–C, unprecedented picoline-derived meroterpenoids from the ascidian-derived fungus *Amphichorda felina* SYSU-MS7908. *Chin. Chem. Lett.* **2021**, *2021*, 1893–1896. [[CrossRef](#)]
20. Chen, S.; Jiang, M.; Chen, B.; Salaenoi, J.; Niaz, S.-I.; He, J.; Liu, L. Penicamide A, A Unique *N*, *N'*-Ketal Quinazolinone Alkaloid from Ascidian-Derived Fungus *Penicillium* sp. 4829. *Mar. Drugs* **2019**, *17*, 522. [[CrossRef](#)]
21. Chen, S.; Guo, H.; Jiang, M.; Wu, Q.; Li, J.; Shen, H.; Liu, L. Mono- and Dimeric Xanthonones with Anti-Glioma and Anti-Inflammatory Activities from the Ascidian-Derived Fungus *Diaporthe* sp. SYSU-MS4722. *Mar. Drugs* **2022**, *20*, 51. [[CrossRef](#)]
22. Hammerschmidt, L.; Debbab, A.; Ngoc, T.D.; Wray, V.; Hemphil, C.P.; Lin, W.; Broetz-Oesterhelt, H.; Kassack, M.U.; Proksch, P.; Aly, A.H. Polyketides from the mangrove-derived endophytic fungus *Acremonium strictum*. *Tetrahedron Lett.* **2014**, *55*, 3463–3468. [[CrossRef](#)]
23. Avent, A.G.; Hanson, J.R.; Truneh, A. Two pyrones from *Gliocladium vermoeseni*. *Phytochem. Lett.* **1992**, *31*, 1065–1066. [[CrossRef](#)]
24. Krick, A.; Kehraus, S.; Gerhäuser, C.; Klimo, K.; Nieger, M.; Maier, A.; Fiebig, H.-H.; Atodiresei, I.; Raabe, G.; Fleischhauer, J. Potential cancer chemopreventive in vitro activities of monomeric xanthone derivatives from the marine algicolous fungus *Monodictys putredinis*. *J. Nat. Prod.* **2007**, *70*, 353–360. [[CrossRef](#)]
25. Liu, B.; Wang, H.-F.; Zhang, L.-H.; Liu, F.; He, F.-J.; Bai, J.; Hua, H.-M.; Chen, G.; Pei, Y.-H. Isolation of a new compound from *Penicillium oxalicum*. *Chem. Nat. Comp.* **2016**, *52*, 821–823. [[CrossRef](#)]

26. Harper, J.K.; Arif, A.M.; Ford, E.J.; Strobel, G.A.; Porco Jr, J.A.; Tomer, D.P.; O'Neill, K.L.; Heider, E.M.; Grant, D.M. Pestacin: A 1, 3-dihydro isobenzofuran from *Pestalotiopsis microspora* possessing antioxidant and antimycotic activities. *Tetrahedron* **2003**, *59*, 2471–2476. [[CrossRef](#)]
27. Li, W.-S.; Hu, H.-B.; Huang, Z.-H.; Yan, R.-J.; Tian, L.-W.; Wu, J. Phomopsols A and B from the mangrove endophytic fungus *Phomopsis* sp. xy21: Structures, neuroprotective effects, and biogenetic relationships. *Org. Lett.* **2019**, *21*, 7919–7922. [[CrossRef](#)]
28. Kendall, J.K.; Fisher, T.H.; Schultz, H.P.; Schultz, T.P. An improved synthesis of 6, 8-dimethoxy-3-methylisocoumarin, a fungal metabolite precursor. *J. Org. Chem.* **1989**, *54*, 4218–4220. [[CrossRef](#)]
29. Wang, H.-H.; Li, G.; Peng, X.-P.; Lou, H.-X. Secondary metabolites from *Colletotrichum fioriniae* F18, an endophytic fungus isolated from the medicinal plant *Mahonia fortunei*. *Acta Pharm. Sin.* **2018**, *12*, 1862–1867.
30. Dimitrios, B. Sources of natural phenolic antioxidants. *Trends Food Sci. Technol.* **2006**, *17*, 505–512. [[CrossRef](#)]
31. Frisch, M.J.; Trucks, G.W.; Schlegel, H.B.; Scuseria, G.E.; Robb, M.A.; Cheeseman, M.A.; Scalmani, G.; Barone, V.; Mennucci, B.; Petersson, G.A.; et al. *Gaussian 09*; Gaussian, Inc.: Wallingford, CT, USA, 2009.
32. Chai, J.-D.; Head-Gordon, M. Long-range corrected hybrid density functionals with damped atom–atom dispersion corrections. *Phys. Chem. Chem. Phys.* **2008**, *10*, 6615–6620. [[CrossRef](#)]
33. Schäfer, A.; Huber, C.; Ahlrichs, R. Fully optimized contracted Gaussian basis sets of triple zeta valence quality for atoms Li to Kr. *J. Chem. Phys.* **1994**, *100*, 5829–5835. [[CrossRef](#)]
34. Zhao, Y.; Truhlar, D.G. The M06 suite of density functionals for main group thermochemistry, thermochemical kinetics, noncovalent interactions, excited states, and transition elements: Two new functionals and systematic testing of four M06-class functionals and 12 other functionals. *Theor. Chem. Acc.* **2008**, *120*, 215–241.
35. Weigend, F.; Ahlrichs, R. Balanced basis sets of split valence, triple zeta valence and quadruple zeta valence quality for H to Rn: Design and assessment of accuracy. *Phys. Chem. Chem. Phys.* **2005**, *7*, 3297–3305. [[CrossRef](#)]
36. Lu, T.; Chen, Q. Shermo: A general code for calculating molecular thermochemistry properties. *Comput. Theor. Chem. Acc.* **2021**, *1200*, 113249. [[CrossRef](#)]
37. Bruhn, T.; Schaumlöffel, A.; Hemberger, Y.; Bringmann, G. SpecDis: Quantifying the comparison of calculated and experimental electronic circular dichroism spectra. *Chirality* **2013**, *25*, 243–249. [[CrossRef](#)]
38. Guo, H.; Wu, Q.; Chen, D.; Jiang, M.; Chen, B.; Lu, Y.; Li, J.; Liu, L.; Chen, S. Absolute configuration of polypropionate derivatives: Decemprones A–J and their MptpA inhibition and anti-inflammatory activities. *Bioorg. Chem.* **2021**, *115*, 105156. [[CrossRef](#)]